This work was written as part of one of the author's official duties as an Employee of the United States Government and is therefore a work of the United States Government. In accordance with 17 U.S.C. 105, no copyright protection is available for such works under U.S. Law.

Public Domain Mark 1.0
https://creativecommons.org/publicdomain/mark/1.0/

Access to this work was provided by the University of Maryland, Baltimore County (UMBC) ScholarWorks@UMBC digital repository on the Maryland Shared Open Access (MD-SOAR) platform.

Please provide feedback

Please support the ScholarWorks@UMBC repository by emailing scholarworks-group@umbc.edu and telling us what having access to this work means to you and why it's important to you. Thank you.

Occurrence, liquid water content, and fraction of supercooled water clouds from combined CALIOP/IIR/MODIS measurements

Yongxiang Hu,[1] Sharon Rodier,[1] Kuan-man Xu,[1] Wenbo Sun,[1] Jianping Huang,[1] Bing Lin,[1] Pengwang Zhai,[1] and Damien Josset[1]

Received 30 April 2009; revised 5 February 2010; accepted 6 May 2010; published 7 October 2010.

[1] The CALIOP depolarization measurements, combined with backscatter intensity measurements, are effective in discriminating between water clouds and ice clouds. The same depolarization measurements can also be used for estimating liquid water content information. Using cloud temperature information from the collocated infrared imaging radiometer measurements and cloud water paths from collocated MODIS measurements, this study compiles global statistics of the occurrence frequency, liquid water content, liquid water path, and their temperature dependence. For clouds with temperatures between −40°C and 0°C, the liquid phase fractions and liquid water paths are significantly higher than the ones from previous studies using passive remote sensing measurements. At midlatitudes, the occurrence of liquid phase clouds at temperatures between −40°C and 0°C depends jointly on both cloud height and cloud temperature. At high latitudes, more than 95% of low-level clouds with temperatures between −40°C and 0°C are water clouds. Supercooled water clouds are mostly observed over ocean near the storm-track regions and high-latitude regions. Supercooled water clouds over land are observed in the Northern Hemisphere over Europe, East Asia, and North America, and these are the supercooled water clouds with highest liquid water contents. The liquid water content of all supercooled water clouds is characterized by a Gamma (Γ) distribution. The mode values of liquid water content are around 0.06 g/m^3 and are independent of cloud temperature. For temperatures warmer than −15°C, mean value of the liquid water content is around 0.14 g/m^3. As the temperature decreases, the mean cloud liquid water content also decreases. These results will benefit cloud models and cloud parameterizations used in climate models in improving their ice-phase microphysics parameterizations and the aviation hazard forecast.

Citation: Hu, Y., S. Rodier, K. Xu, W. Sun, J. Huang, B. Lin, P. Zhai, and D. Josset (2010), Occurrence, liquid water content, and fraction of supercooled water clouds from combined CALIOP/IIR/MODIS measurements, *J. Geophys. Res.*, *115*, D00H34, doi:10.1029/2009JD012384.

1. Introduction

[2] It is well known that supercooled water clouds exist in both stratiform clouds and convective clouds with temperature lower than 0°C. Supercooled water has been found in stratiform clouds between 40°S and 60°S from Lidar In-space Technology Experiment (LITE) data analysis [*Hogan et al.*, 2004]. Supercooled water clouds can also be found in the developing stage of the convective cloud life cycle when there are not sufficient numbers of ice nuclei [*Mason*, 1952]. The water-ice mixture of the air parcels in which mixed phase clouds occur varies with time. Liquid water dominates initially due to the abundance of cloud condensation nuclei (CCN) compared to ice nuclei [*Ghan and Easter*, 1992]. Liquid droplets form at the beginning of the cloud life cycle when warm, moist air is cooled by processes such as adiabatic lifting and/or radiative cooling. As the cooling continues, ice nucleation begins through heterogeneous nucleation on dust, biological particles, and other nonsoluble particles. Because of their low saturation vapor pressure, ice crystals will grow at the expense of the supercooled water. During high-latitude winter, supercooled water can also form when warm, moist air flows above a colder boundary layer [*Curry et al.*, 1996], related to strong boundary-layer convection.

[3] The treatment of mixed-phase clouds in the cloud life cycle is an important part of cloud modeling for weather and climate predictions [e.g., *Tao*, 2003; *Toon et al.*, 1989]. When water droplets convert into ice crystals, the cloud layer becomes optically thinner because the ice cloud layer contains fewer and larger ice particles and the scattering cross section is reduced. This difference in optical depth affects radiative heating and energy balance. Ice also absorbs more in the near infrared wavelengths than water clouds. Furthermore, parameterization of the cloud phase also plays a critical

[1]Climate Science Branch, NASA Langley Research Center, Hampton, Virginia, USA.

This paper is not subject to U.S. Copyright.
Published in 2010 by the American Geophysical Union.
0148-0227/10/2009JD012384

role in determining climate feedbacks [*Li and Le Treut*, 1992]. With the increase in greenhouse gases, general circulation model (GCM)-simulated storm tracks move poleward [*Yin*, 2005] and so too do the associated water clouds. It has been found that many of the clouds within storm tracks are supercooled water clouds [*Hogan et al.*, 2004]. When water clouds move poleward, the reduction of solar insulation at higher latitudes causes a concomitant reduction in global albedo. A recent GCM intercomparison study indicates that the difference in albedo feedback among different models is primarily a result of the differences in the poleward redistribution of cloud liquid water due to differences in mixed-phase cloud algorithms [*Tsushima at al.*, 2006]: the models that produce more supercooled water clouds have a higher sensitivity. Global statistics of cloud phase observations for cloud temperature between −40°C and 0°C can therefore be used to constrain the GCM cloud parameterizations and thus help reduce uncertainties in cloud feedbacks.

[4] Using both layer-integrated backscatter and depolarization ratio, cloud phase can be determined by CALIOP measurements [*Hu et al.*, 2001, 2009; *Hu*, 2007]. For stratiform clouds and convective clouds with cloud optical depths greater than 0.5, the cloud temperature can be estimated reasonably well using the combination of CALIPSO infrared imaging radiometer (IIR) measurements and lidar measurements. Cloud temperature can also be estimated from temperature profiles of GEOS-5 data assimilation product together with CALIOP cloud height measurements. The global statistics of the combined measurements are analyzed for estimating the probability of supercooled water cloud occurrence as a function of cloud temperature. Because single scattering from spherical particles will not depolarize the lidar backscatter signal, water cloud depolarization from CALIOP is caused by multiple scattering and can be used to estimate cloud liquid water content near cloud top [*Hu et al.*, 2007a]. This study also analyzes the cloud liquid water content as a function of cloud temperature using the combined CALIOP and IIR measurements.

2. Cloud Temperature and Cloud Phase from CALIOP and IIR Measurements

[5] This study is based on the analysis of CALIPSO [*Winker et al.*, 2007] Level 2, version 2.01 nighttime 5 km cloud layer products and the collocated IIR level 1 temperatures for a time period spanning January 2008 to December 2008. During this time period, CALIOP is tilted 3° off-nadir to avoid specular reflection from horizontally oriented ice particles from contaminating the cloud phase discrimination and retrievals of ice cloud optical depths [*Hu*, 2007; *Hu et al.*, 2007c]. In this study, we only consider the first layer detected by CALIOP since the temperature of these clouds can be accurately estimated from IIR measurements. Broken clouds smaller than 5 km are not considered in this study. Preliminary studies with higher resolution CALIPSO data indicate that the impact of broken clouds on supercooled water cloud statistics is limited.

[6] A specialized cloud thermodynamic phase product is developed for this study. The cloud phase product is based on the measurements of cloud backscatter, depolarization, and their spatial coherence [*Hu*, 2007; *Hu et al.*, 2006, 2009]. The current CALIPSO cloud thermodynamic phase discrimination is based on the depolarization of backscattered light measured by its lidar (CALIOP). It assumes that backscattered light from ice crystals is depolarizing, whereas water clouds, being spherical, result in minimal depolarization. However, because of the relationship between the CALIOP field of view (FOV) and the large distance between the satellite and clouds and because of the frequent presence of oriented ice crystals, the measured depolarization ratios of ice clouds sometimes can be less than those of water clouds, which thereby creates significant uncertainties in the current CALIOP phase determination. For water clouds, the CALIOP-measured depolarization can be large due to multiple scattering, whereas horizontally oriented ice particles depolarize only weakly and behave similarly to water clouds. Because of the nonunique depolarization–cloud phase relationship, more constraints are necessary to uniquely determine cloud phase. Based on theoretical and modeling studies, an improved cloud phase determination algorithm has been developed. Rather than depending primarily on layer-integrated depolarization ratios, this algorithm differentiates cloud phases by using the spatial correlation of layer-integrated attenuated backscatter and layer-integrated particulate depolarization ratio. This approach includes a two-step process: (1) use of a simple two-dimensional threshold method to provide a preliminary identification of ice clouds containing randomly oriented particles, ice clouds with horizontally oriented particles, and possible water clouds and (2) application of a spatial coherence analysis technique to separate water clouds from ice clouds containing horizontally oriented ice particles. Other information, such as temperature, color ratio, and vertical variation of depolarization ratio, is also considered. The algorithm differentiates water cloud droplets from ice clouds composed of randomly oriented particles, as well as ice cloud with horizontally oriented particles. The algorithm works well for both the 0.3° and 3° off-nadir lidar pointing geometry [*Hu et al.*, 2009]. As with passive remote sensing instruments, mixed-phased clouds with high optical depths can be misidentified by CALIOP, since CALIOP is more sensitive to the clouds in the top range bins with optical depth around 3, and backscatter by water clouds is significantly stronger than backscatter by ice clouds for the same water content. For this study, the water clouds are those clouds that are predominantly water in the top 3 optical depths.

[7] IIR cloud temperature is derived from collocated lidar and IIR measurement. Surface contribution to the IIR radiances are corrected with cloud optical depth derived from CALIPSO and GEOS-5 ocean/land surface temperature. The contribution of water vapor to IIR radiance is corrected with GEOS-5 atmospheric water vapor and temperature profiles [*Dubuisson et al.*, 2005].

[8] Cloud liquid water content is computed from water cloud depolarization and collocated MODIS cloud droplet size measurements [*Hu et al.*, 2007a]. Cloud liquid water content (LWC) can be derived from cloud extinction coefficient (β) and water droplet effective radius (Re) [*Hu and Stamnes*, 1993] using the equation $\mathrm{LWC} = \frac{2}{3\rho} * \beta * \mathrm{Re}$. Here ρ is the density of water. The depolarization of lidar backscatter from water clouds is caused by multiple scattering. The multiple scattering depends on extinction coefficient and droplet size. Using Monte Carlo simulations, a simple empirical relation linking the extinction coefficient (β), the

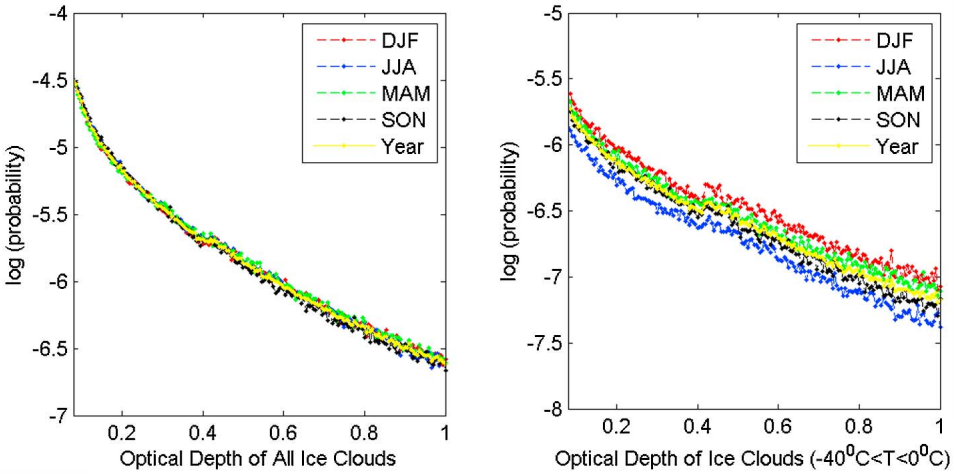

Figure 1. Probability distribution of 532 nm cloud optical depth (left) for all ice clouds and (right) for ice clouds with temperature between −40°C and 0°C. The ice cloud optical depth is estimated from layer-integrated attenuated backscatter using fixed effective lidar ratio of 17 [*Hu*, 2007].

depolarization ratio (δ), and the effective radius (Re) of water clouds is established [*Hu et al.*, 2007a; 2007b]. This relation is adopted in this study to derive water cloud extinction coefficients from the lidar measurements of depolarization ratios and the collocated MODIS measurements of effective radii.

[9] Mid-layer cloud temperature is estimated from CALIOP cloud height measurements and GEOS-5 temperature profiles.

[10] As supercooled water clouds appear primarily in stratiform, congestus, and convective clouds, we need to select lidar backscatter thresholds in order to remove irrelevant thin cirrus clouds and prevent them from contaminating the statistical analysis of the supercooled water clouds. The number of ice cloud cases detected by CALIOP increases exponentially with decreasing ice cloud optical depth, and the optical depth distributions for different seasons are nearly identical (Figure 1, left).

[11] Ice clouds appear colder during June, July, and August (JJA) than in other seasons (Figure 2). Ice clouds opaque to CALIOP have similar temperature distributions in different seasons (Figure 2, right). The thin ice clouds are colder in June, July, and August than in December, January, and February (Figure 2), thus we see fewer thin ice clouds with cloud temperature warmer than −40°C in June, July, and August (Figure 1, right).

[12] Most of the thin cirrus clouds with optical depth less than 0.4 are in the upper troposphere and have temperatures colder than −40°C (Figure 3, left). Thin cirrus clouds in the temperature range between −40°C and 0°C appear less frequently than clouds at lower temperatures (Figures 1 and 3), and these thin warmer cirrus clouds are not the subjects of interest (i.e., convective clouds or the stratiform) of this study. Assuming an effective lidar ratio of 17 sr [*Hu*, 2007], the layer-integrated attenuated backscatter for a layer of ice clouds with optical depth 0.4 is ~0.01 sr^{-1}. In this study, we consider only those clouds with layer-integrated attenuated backscatters greater than 0.01 sr^{-1} (i.e., optical depths greater than 0.4). The thinner ice clouds are ignored for other

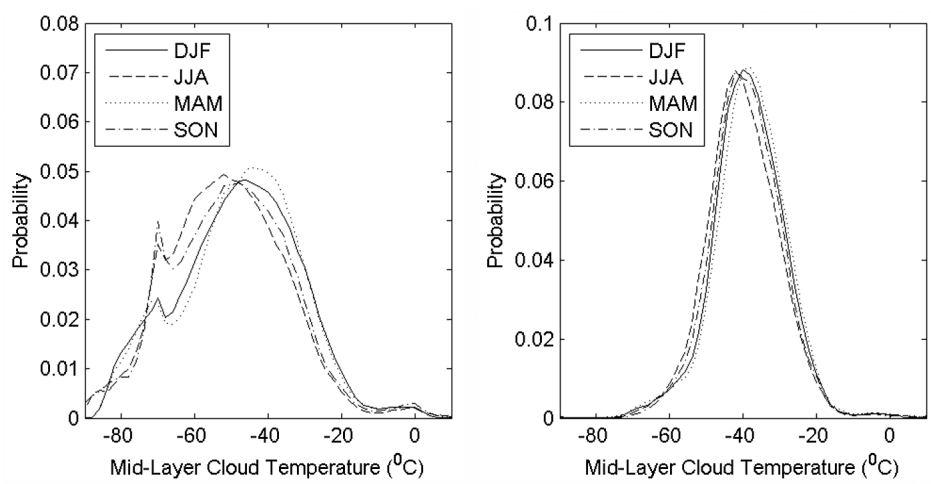

Figure 2. Seasonal dependence of cloud temperature for (left) non-opaque ice clouds and (right) opaque ice clouds.

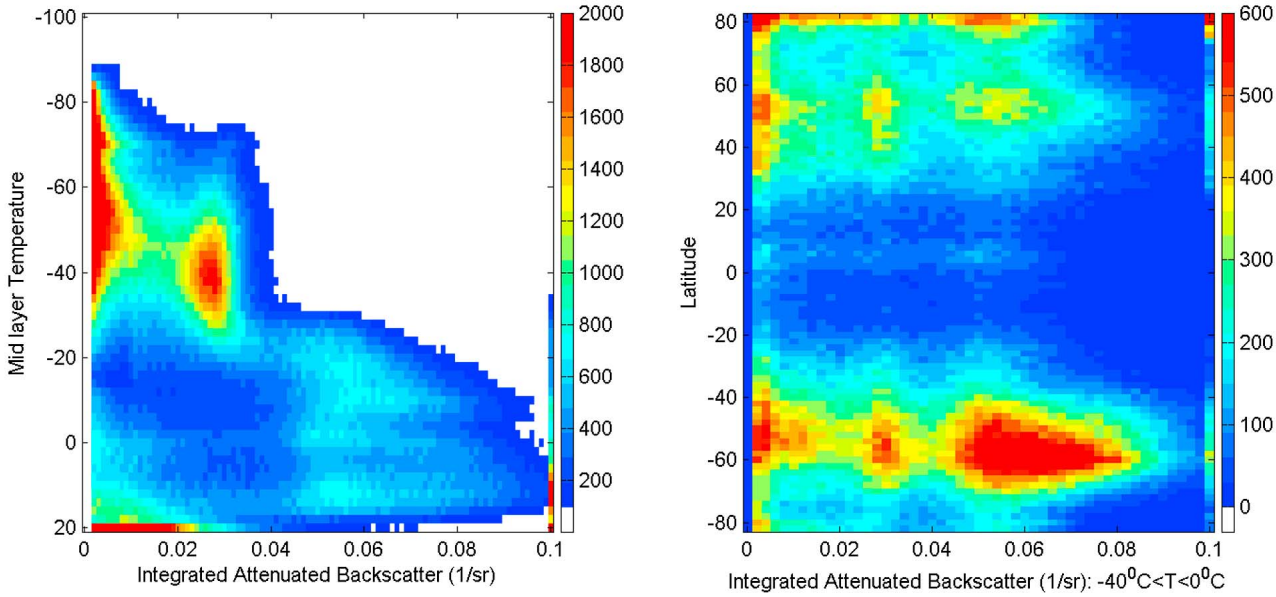

Figure 3. Frequency of occurrence for (left) clouds with various temperature and cloud layer-integrated attenuated backscatter and (right) latitudinal distribution of clouds with mid-layer temperature between −40°C and 0°C.

practical reasons as well. It is more difficult to determine their cloud phase due to the low signal-to-noise ratios (SNR) of the lidar measurements, and it is also more difficult to determine the accuracy of cloud temperature estimation from the IIR brightness temperature measurements. There has been some dust considered as clouds in the CALIPSO Version 2 lidar product. As dust aerosol backscatters less than ice clouds, some of the warm and thin "clouds" (Figure 3, left) may be thick dust aerosols. Most thin clouds with backscatter less than 0.01 sr^{-1} are ice clouds colder than −30°C or a misidentified dust layer. By ignoring thin clouds with backscatter less than 0.01 sr^{-1}, our statistics will be less affected by these misidentified dust layers. On the other hand, a fraction of the clouds with layer-integrated backscatter less than 0.01 sr^{-1} that is not considered in this study can be optically thin ice or water clouds, such as part of the altocumulus clouds observed in tropical regions [*Ansmann et al.*, 2009]. Broken cloud missing from the 5 km CALIPSO data product is another group of clouds that are not represented here. Other parameters, such as cloud geometric depth and temperature agreement between GEOS-5 and IIR temperatures, were not used as criteria for selection.

[13] Two different sources of cloud temperature are considered in this study: (1) mid-layer cloud temperature estimated from GEOS-5 temperature profile and CALIOP cloud height and (2) cloud temperature estimated from IIR measurements at 10.8 μm channel after correcting for gaseous absorption and emission. The two temperature estimates for water clouds fall within 3°C of each other over most regions of the Earth (Figure 4, top). For ice clouds, IIR cloud temperatures are generally 5°C to 7°C higher than the mid-layer temperatures outside of the tropics and IIR cloud temperatures are as much as 20°C higher than the mid-layer temperatures in the tropical region (Figure 4, bottom).

[14] The reasons why IIR ice cloud temperatures in the tropics are higher include: (1) IIR temperatures are weighted more toward the lower part of the ice cloud layer; (2) for non-opaque ice clouds, thermal emissions from the surface and/or lower level clouds may transmit through the ice cloud layer, resulting in an ice cloud layer that appears to be warmer than it actually is; (3) cloud temperature can be higher than air temperature derived from GEOS-5 assimilation; and (4) there are uncertainties in data assimilation which affect GEOS-5 temperature profiles. The large difference between the two temperature estimates in the tropics holds for opaque ice clouds as well.

[15] For mid-layer temperatures within the −20°C to 0°C range, more than 75% of the clouds with layer-integrated attenuated backscatters lower than 0.02 sr^{-1} are water clouds (Figure 5, left). On the other hand, for IIR cloud temperature between −20°C and 0°C, less than 30% of clouds with attenuated backscatter lower than 0.02 sr^{-1} are water clouds (Figure 5, right). This difference may be due to thin ice clouds that are interpreted as being warmer than they actually are or to the ice clouds that are warmer than the air temperatures derived from GEOS-5 assimilation. The results shown in Figure 5 (right) are consistent from a radiative transfer perspective. It is expected that backscatter by ice clouds will, in general, be weaker than backscatter from water clouds [*Hogan et al.*, 2004]. For the same scattering cross section, backscatter cross sections of water clouds are nearly twice as big as ice clouds. Multiple scattering contributes to about 70% of CALIOP water cloud backscatter signal [*Hu*, 2007] and about half of CALIOP ice cloud backscatter [*Hu et al.*, 2007c]. For the same single-scattering optical depths, CALIOP water cloud backscatter is twice to three times as large as ice cloud backscatter.

3. Fraction of Supercooled Water Clouds

[16] Using the CALIOP cloud phase measurements and the two different cloud temperature estimates, the fractions

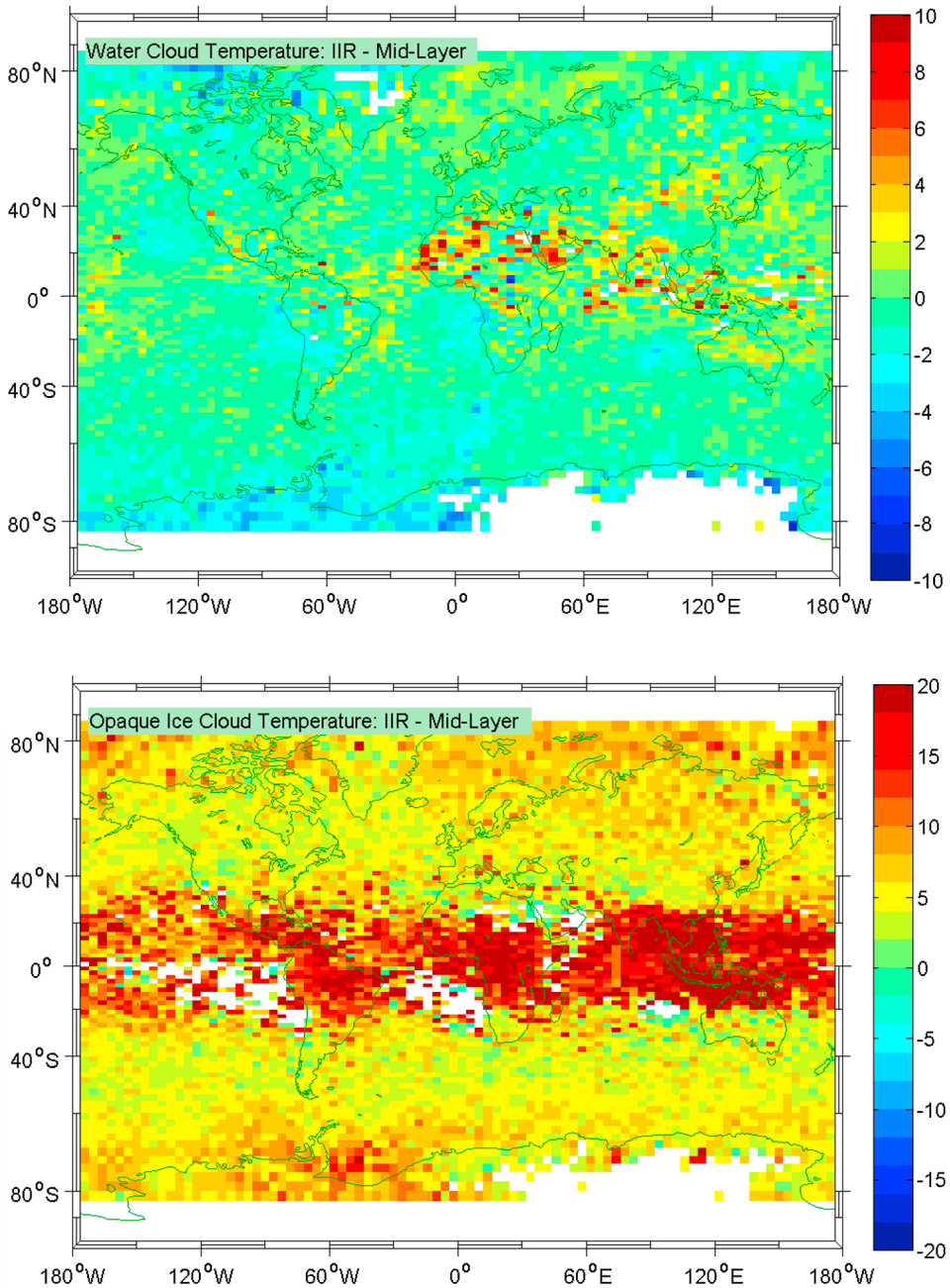

Figure 4. Cloud temperature differences (°C) between IIR measurements and estimated from GEOS-5 temperature profiles with lidar cloud height: (top) water clouds; (bottom) ice clouds.

of supercooled water clouds are plotted against cloud temperatures (Figures 6a through 6d). Supercooled water clouds are rarely found below −35°C, which is consistent with the results obtained from the LITE measurements [*Hogan et al.*, 2004]. The relation between the fraction of supercooled water clouds and mid-layer temperature in terms of global statistics (Figure 6a) has very little seasonal variation, except for June, July, and August. Ice clouds are rare for mid-layer temperature warmer than −15°C. On the other hand, a small fraction of ice clouds can be seen with IIR temperatures between −15°C and 0°C (Figure 6b).

[17] The relation between the fraction of supercooled water clouds and cloud temperature can be parameterized with sigmoid function,

$$f(T) = \frac{1}{1 + e^{-p(T)}}. \tag{1}$$

[18] Here $p(T)$ is a polynomial fit to the observed relations between fraction of supercooled water presence $f(T)$ and temperature as shown in Figure 6. This relation is different from the ones used in cloud microphysics parameterizations

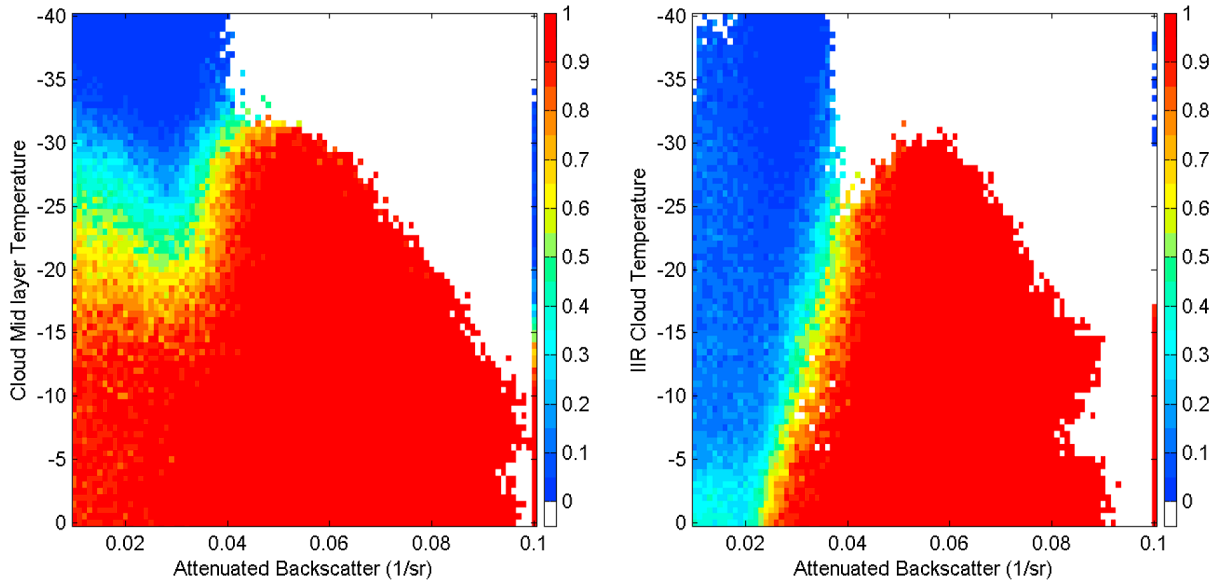

Figure 5. Probability of the cloud being supercooled water phase: its relation to mid-layer cloud temperature (left), as well as its relation to IIR brightness temperature (right) for various integrated attenuated backscatters.

of climate models [see *Klein et al.*, 2009], which is typically piecewise linear between the low and upper temperature thresholds. The least squares fit of $p(T)$, for mid-layer cloud temperature T_{mid} (dotted line of Figure 6a) and IIR temperature T_{IIR} (dotted line of Figure 6b), are

$$p(T_{\mathrm{mid}}) = 5.3608 + 0.4025T_{\mathrm{mid}} + 0.08387T_{\mathrm{mid}}^2 + 0.007182T_{\mathrm{mid}}^3 + 2.39 \times 10^{-4}T_{\mathrm{mid}}^4 + 2.87 \times 10^{-6}T_{\mathrm{mid}}^5, \quad (2)$$

$$p(T_{\mathrm{IIR}}) = 5.2918 + 0.3694T_{\mathrm{IIR}} + 0.06635T_{\mathrm{IIR}}^2 + 0.006367T_{\mathrm{IIR}}^3 + 2.33 \times 10^{-4}T_{\mathrm{IIR}}^4 + 2.97 \times 10^{-6}T_{\mathrm{IIR}}^5. \quad (3)$$

The fraction of supercooled water presence over ocean is larger than over land (Figure 6c). The fraction of supercooled water presence is highest over higher latitude snow/ice-covered surfaces.

[19] It is important to note that the CALIPSO statistics in Figures 6a through 6d are the fraction of supercooled water presence, whereas what is important for cloud parameterizations is the statistics of supercooled water path. In order to derive the statistics of supercooled water path from the statistics of supercooled water presence, ice water and liquid water paths from collocated MODIS observations in the CERES SSF data product [*Lin and Rossow*, 1994, 1996; *Ho et al.*, 2003] are adopted in this study.

[20] On average, the ice water path of an ice cloud can be significantly larger than the liquid water path of a water cloud layer at the same cloud temperature (Figure 6e), and the difference increases while temperature decreases. Combining the MODIS mean ice water and liquid water paths with the fraction of supercooled water presence from CALIPSO, we can estimate the fraction of the supercooled water path (Figure 6f). The relation between the fraction of supercooled water path and cloud temperature can be also parameterized with a sigmoid function (Red solid line of Figure 6d). The $p(T)$ value in the sigmoid function (Equation 1) is

$$p_{\mathrm{path}}(T_{\mathrm{IIR}}) = 7.6725 + 1.0118T_{\mathrm{IIR}} + 0.1422T_{\mathrm{IIR}}^2 + 0.0106T_{\mathrm{IIR}}^3 + 3.39 \times 10^{-4}T_{\mathrm{IIR}}^4 + 3.95 \times 10^{-6}T_{\mathrm{IIR}}^5. \quad (4)$$

The fraction of supercooled water path from CALIPSO measurements is compared with values in existing models and from previous observations [e.g., *Smith*, 1990; *Del Genio et al.*, 1996; *Lin and Rossow*, 1996; *Weidle and Wernli*, 2008] of Figure 6d. For clouds with temperature between −15°C and −25°C, the parameterization from CALIPSO data has a greater quantity of supercooled water than all other parameterizations.

[21] It is possible that ice water paths for clouds with temperature between 0°C and −40°C in previous studies were significantly overestimated due to an overestimation of ice cloud optical depths from passive remote sensing and uncertainties associated with multilayer clouds. Recent studies indicate that MODIS ice cloud optical depths are twice as much as CALIPSO optical depths (R. Holz, personal communication, 2009). The overestimation of ice cloud optical depths, combined with the likelihood of optically thin, cold ice clouds over warm water clouds that are identified as middle-level ice clouds with high optical depths, may cause significant overestimation of global ice water paths of clouds with temperature between 0°C and −40°C.

[22] There are potential error sources in the CALIPSO statistics. Both the lidar backscatter and the infrared emission are most sensitive to the top 2 to 3 optical depths of the atmosphere. The phase of a layer of mixed-phase cloud can be misidentified as either water or ice, depending on what dominates the signal of the top optical depths. Since only the top cloud layer is considered in this study, the statistics may be biased toward higher altitude clouds. Thus, the fraction of

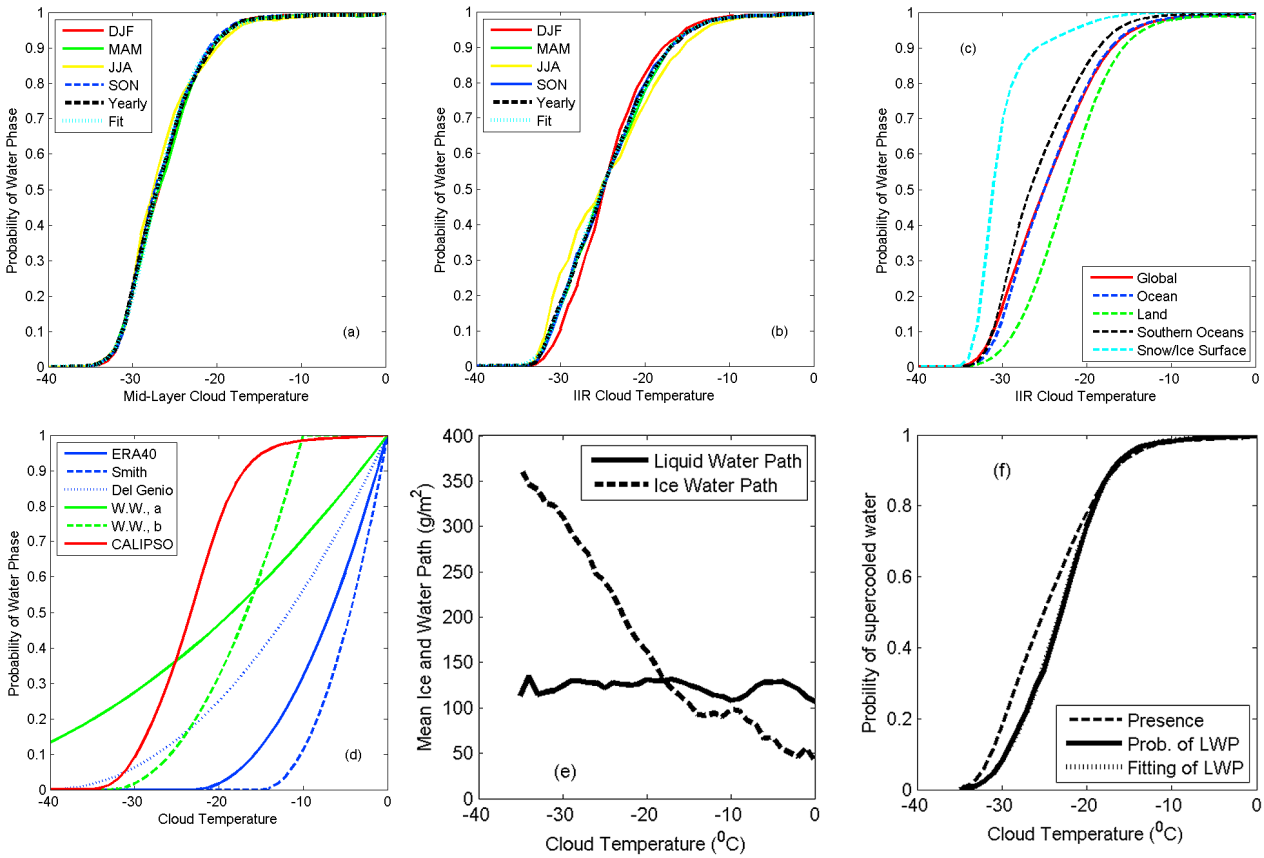

Figure 6. Relation between cloud temperature and fraction of supercooled water clouds. (a) Seasonal variation using the mid-layer cloud temperature as reference. (b) Seasonal variation using IIR cloud temperature as reference. (c) Probability of supercooled water clouds with IIR cloud temperature as a reference for observations found globally, over ocean, over land and snow and ice surfaces. (d) Comparisons of the fractions of supercooled water path with existing models and observations (red solid line, CALIPSO observation; blue solid line, ERA40 data; blue dashed line, data from *Smith* [1990]; blue dotted line, data from *Del Genio et al.* [1996]; green lines, polarimeter data from *Weidle and Wernli* [2008]). (e) Mean liquid and ice water path from collocated MODIS observations in CERES product. (f) Fraction of supercooled water path (solid) and the polynomial fit(s) (dotted).

supercooled water presence may be underestimated since the fraction of supercooled water presence has altitude dependence (Figure 8), especially at high latitudes.

[23] The goal of this study is not to develop a parameterization for the relationship between the supercooled water fraction and temperature that is valid for the entire globe. It is, however, important to understand the variability of this relationship so that a physically based cloud microphysics parameterization in climate models or cloud models can reproduce the observed relationship. First, we notice that the relationship between the supercooled water fraction and cloud temperature shows a latitudinal dependency (Figure 7). For the same mid-layer cloud temperature, the fraction of supercooled water is higher at higher latitudes than at lower latitudes (Figure 7, left). The relationship between supercooled water fraction and IIR temperature shows a similar latitudinal dependence (Figure 7, right).

[24] Besides the dependence on temperature and latitude, the fraction of supercooled water is also a function of cloud height (Figure 8a), especially at higher latitudes (Figure 8d) and in the tropics (Figure 8b). In the tropics, the fraction of supercooled water is always higher than 95% for clouds below 8 km. For higher latitudes, the dependence of supercooled water presence on cloud height is as strong as that on cloud temperature.

[25] Compared with existing parameterization [*Klein et al.*, 2009], many more supercooled water clouds are observed by the CALIOP measurements. This is reflected in our new parameterization (equation (1)–(3)), because the parameterization weights all observations equally and most supercooled clouds are in the high-latitude regions where supercooled water fraction is higher.

4. Distribution of Supercooled Water Cloud Occurrence and Liquid Water Content

[26] To further understand the different dependences of supercooled water presence on cloud height in different latitudinal bands (Figure 8) and the supporting physics, the

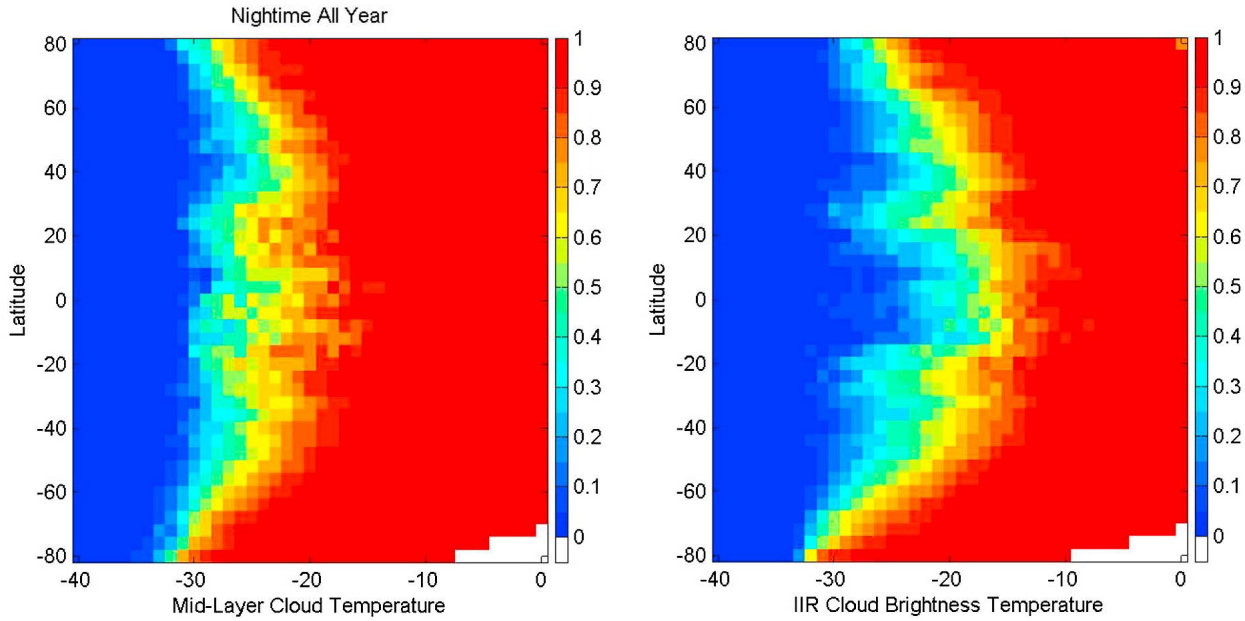

Figure 7. Latitudinal and temperature dependence of supercooled water probability: (left) using mid-layer cloud temperature as reference; (right) using IIR cloud temperature as reference.

preferred geographic locations of the supercooled cloud occurrence and liquid water contents are examined. Figure 9 (top) shows where the supercooled water clouds are observed and the color represents the number of times supercooled water clouds are observed by CALIOP during 2008 within each 2° latitude by 3° longitude grid boxes. Most supercooled water clouds are located near the storm track regions over the Southern Ocean, North Pacific Ocean, and North Atlantic Ocean. However, there are fewer supercooled water clouds observed over land. Most supercooled water clouds over land are in Europe, East Asia, and North America. The presence of supercooled water clouds is very low between 40°S and 40°N, except over China (Figure 9, top).

[27] In storm track, polar region and East Asia region, more than 70% of clouds with temperature between 0°C and −40°C are supercooled water clouds (Figure 9, bottom).

[28] The supercooled water clouds occurring over land have high liquid water content (Figure 10, top). The highest liquid water contents of supercooled water clouds are seen in Europe and East Asia. Supercooled water clouds are rarely seen in most of Africa and South America (Figure 9, top). For the few supercooled cloud cases observed, high liquid water contents appear in South American regions such as northern Argentina and Paraguay, and coastal African regions of Namibia, Angola, and Mozambique (Figure 10, top). On average, the liquid water contents of supercooled water clouds are not high as the warm water clouds ($T > 0$°C) of the eastern Pacific off the coasts of North and South Americas, and in the eastern Atlantic off the African coast (Figure 10, bottom). These warm water clouds are associated with marine stratocumulus decks.

[29] Reduction in ice-forming nuclei due to pollution [*Borys*, 1989] may be a cause of the large presence of supercooled water clouds with high liquid water contents in highly populated regions such as Europe and China. Sulfate particles in polluted air may coagulate with ice-forming nuclei and deactivate them [*Curry et al.*, 1996]. Comparing summer and fall seasons, many more supercooled water clouds in China and northern hemispheric storm track are observed during winter and spring seasons. For Southern Ocean, more supercooled water clouds are observed in summer, and their liquid water content in summer is also significantly higher than in winter.

[30] The liquid water content of supercooled water clouds follows a gamma (Γ) distribution with a mode around 0.06 g/m^3 (Figure 11, left) and a mean value of 0.14 g/m^3. This mean value is consistent with in situ measurements of *Korolev et al.* [2007]. With decreasing cloud temperature, it is less likely to find supercooled water clouds with large liquid water contents (Figure 11). It is important to note that we can only derive the liquid water contents of the top portion of the water clouds from CALIOP lidar depolarization ratios and MODIS effective radii.

[31] The joint cloud temperature – cloud liquid water content distribution shows that it is most likely to encounter supercooled water with high liquid water content (higher risk for aviation icing condition) when cloud temperatures are around −10°C (Figure 11, right).

5. Summary

[32] Using the CALIOP cloud phase and cloud height measurements, together with cloud temperature information from the collocated IIR measurements and GEOS-5 assimilation, this study provides the global statistics of the occurrence and temperature dependence of supercooled water clouds. Based on the global statistics from the observations, a sigmoid functional fit for the relationship between the fraction of supercooled water clouds and temperature was

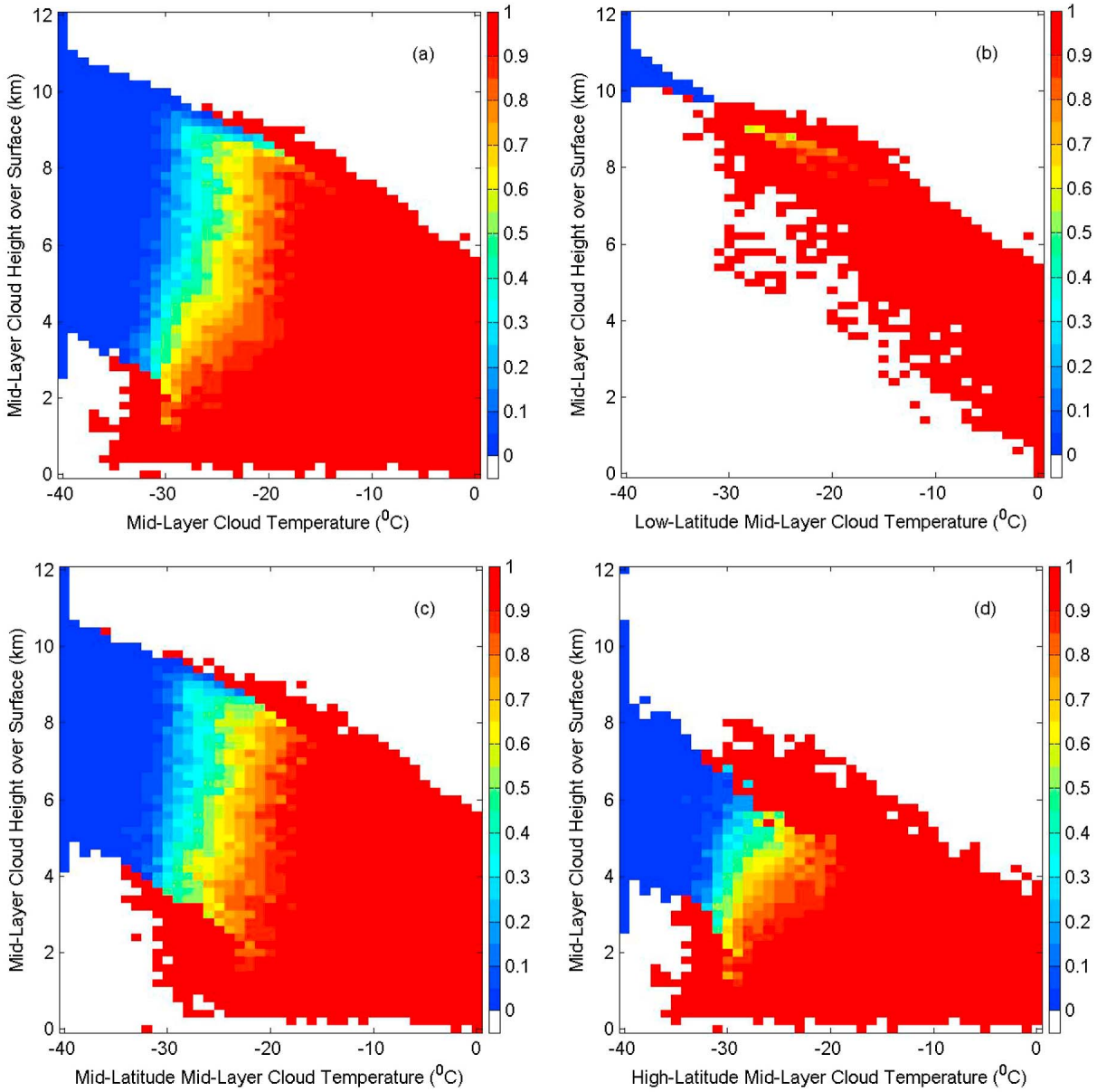

Figure 8. Altitude and temperature dependence of supercooled water probability: (a) combined observations; latitudinal dependence in (b) tropics 20°S–20°N; (c) mid-latitudes 20°N–60°N plus 20°S–60°S; (d) high latitudes 60°N–82N plus 60°S–82°S.

obtained. This relationship is different from the ones presently used in cloud microphysics parameterizations of climate models [see *Klein et al.*, 2009], which is typically piecewise linear between the low and upper threshold temperatures. Compared with existing parameterizations [e.g., *Smith*, 1990; *Del Genio et al.*, 1996; *Klein et al.*, 2009] and previous observations [e.g., *Lin and Rossow*, 1996; *Weidle and Wernli*, 2008], many more supercooled water clouds are observed by the CALIOP measurements. This is reflected in our new parameterization. The parameterization weights all observations equally and most supercooled clouds are in the high-latitude regions where supercooled water fraction is higher. For clouds with temperatures between −15°C and 0°C, the fraction of liquid phase clouds is higher than 95%. There are, however, regional differences in the relationships, and these relationships are dependent on cloud height. The thermodynamic phase of clouds occurring in the middle and high latitudes with temperatures between −40°C and 0°C depends on both cloud height and cloud temperature. At high latitudes, more than 95% of low-level clouds (cloud height lower than 2 km) with temperature between −40°C and 0°C are water clouds. A significant portion of middle-level ice clouds identified by passive remote sensing is made up of thin cold ice clouds over thick warm water clouds. This is one of the reasons for the difference between this study and previous studies based on passive remote sensing data.

[33] Supercooled water is mostly observed in clouds over middle and high latitudes (40°S–60°S, and 40°N–70°N).

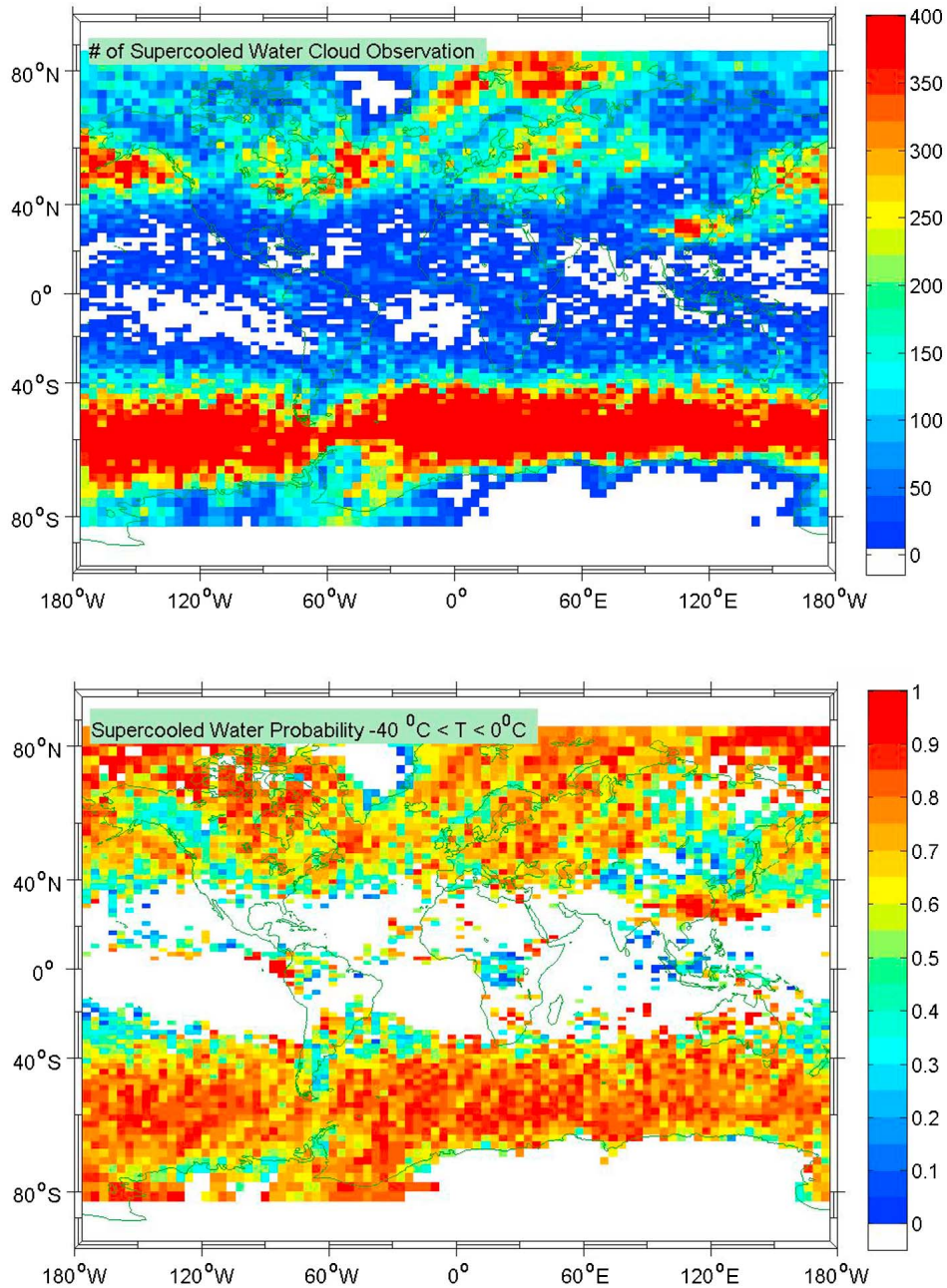

Figure 9. Number of observed supercooled water clouds during 2008 (top) and probability distribution of supercooled water clouds (bottom) for clouds with cloud temperature between 0°C and −40°C.

The only lower latitude region (40°S–40°N) with a large supercooled water presence is eastern Asia. Most supercooled water clouds are closely associated with storm tracks in both hemispheres, with the largest occurrence in the Southern Ocean. Supercooled water clouds are also frequently present over land in such regions in the Northern Hemisphere as Europe, East Asia, and North America. Deactivation of ice-forming nuclei by sulfate particles and dimethylsulfide may be a factor in the regional distribution of the supercooled water cloud occurrence.

[34] Supercooled water clouds in Europe and East Asia (mostly in China) have the highest liquid water contents. Globally, liquid water content of supercooled water clouds follows a gamma distribution, with mode values of liquid water content around 0.06 g/m^3. The mean value of the liquid water content is around 0.14 g/m^3. The temperature associated with the highest liquid water content is −10°C, arising from the longest tail in the gamma distribution.

[35] More theoretical studies, laboratory experiments, and in situ measurements are needed to further understand the cloud microphysics behind the regional and temporal variations of supercooled water cloud occurrence, especially in the highly populated regions and Southern Ocean. More studies are needed to improve the parameterization by combining with more collocated measurements such as CloudSat and Parasol. Future studies are also required to assess the

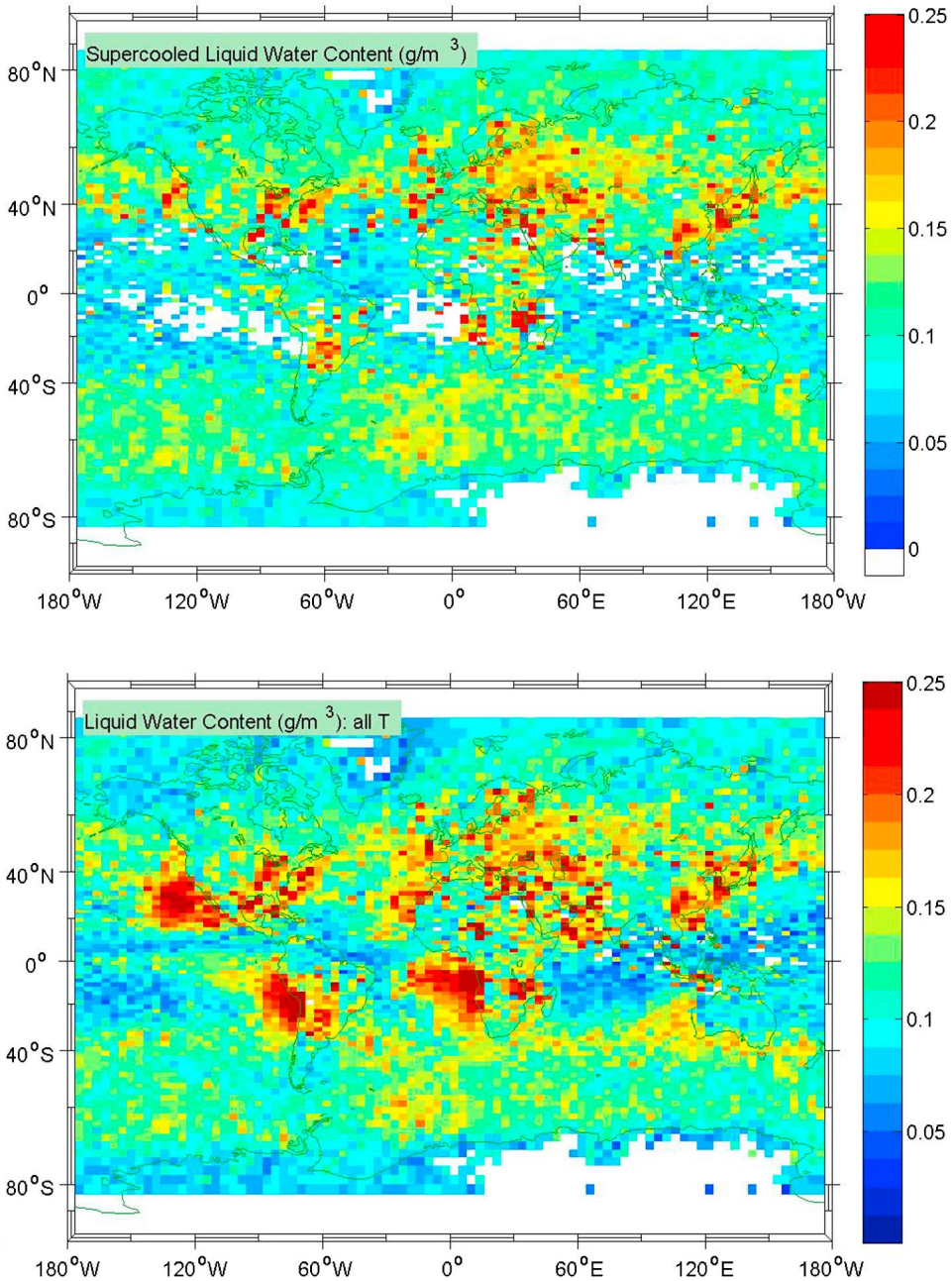

Figure 10. Averaged liquid water content for supercooled water clouds (top) and for water clouds at all temperatures (bottom).

errors associated with the uncertainties of the CALIPSO cloud/aerosol classification, CALIPSO cloud phase discrimination, and cloud ice water path derived from MODIS.

[36] The statistics presented in this study can be helpful to evaluate relationships between the supercooled water fraction and temperature simulated from global climate models. The variability of the relationships over different regions and latitudinal bands, as well as the dependence on cloud height are particularly useful information to improve physically based cloud microphysics parameterizations in climate models or cloud models. These statistics and relationships will also be useful to improve aviation hazard forecast. Passive remote sensing of mixed phase clouds [*Baum et al.*, 2000; *Nasiri and Kahn*, 2008] will also benefit from the CALIOP cloud phase analysis.

[37] Water cloud temperatures derived from GEOS-5 assimilation and CALIOP cloud height measurements agree reasonably well with collocated IIR temperature measurements, suggesting that the assimilated temperature fields from GEOS-5 are reasonably accurate. There is, however, discrepancy between the two temperatures estimates for semitransparent tropical ice clouds, and this discrepancy exists for opaque ice clouds as well. It does not, however, affect the global statistics of supercooled water clouds since supercooled water clouds occur mostly in higher latitudes. The discrepancy can be further analyzed by future studies

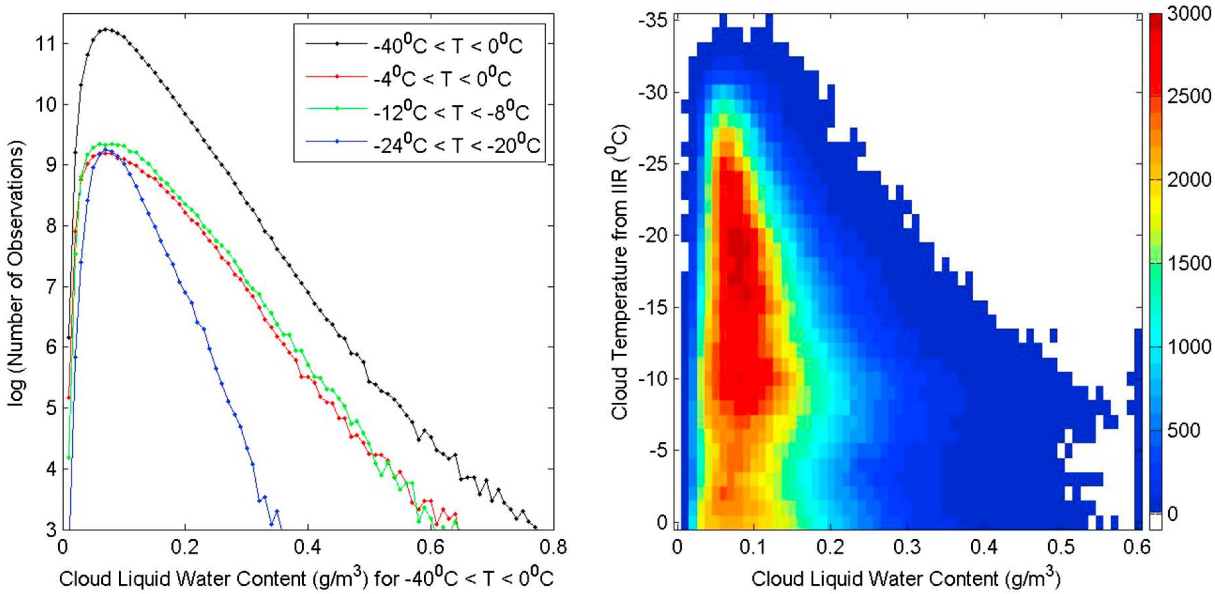

Figure 11. (left) Supercooled water content distributions. Black line is for all supercooled water. Blue, red, and green lines are for three warmer cloud temperature intervals. (right) Same as on the left except for the joint cloud temperature-cloud liquid water content distribution.

using collocated cloud and surface information from MODIS and AMSR-E measurements.

[38] **Acknowledgments.** This work is supported by the NASA radiation science program and CALIPSO project. The manuscript benefited from Mark Vaughan's editorial support. The authors want to also thank Dr. Hal Maring of NASA Headquarters for the discussions and support.

References

Borys, R. D. (1989), Studies of ice nucleation by arctic aerosol on AGASP-II. *J. Atmos. Chem.*, *9*, 169–185.

Ansmann, A., M. Tesche, P. Seifert, D. Althausen, R. Engelmann, J. Fruntke, U. Wandinger, I. Mattis, and D. Müller (2009), Evolution of the ice phase in tropical altocumulus: SAMUM lidar observations over Cape Verde, *J. Geophys. Res.*, *114*, D17208, doi:10.1029/2008JD011659.

Baum, B. A., P. F. Soulen, K. I. Strabala, M. D. King, S. A. Ackerman, W. P. Menzel, and P. Yang (2000), Remote sensing of cloud properties using MODIS airborne simulator imagery during SUCCESS: 2. Cloud thermodynamic phase, *J. Geophys. Res.*, *105*, 11,781–11,792.

Curry, J. A., J. C. Schramn, W. B. Rossow, and D. A. Randall (1996), Overview of Arctic Cloud and Radiation Characteristics, *J. Climate*, *9*, 1731–1764.

Del Genio, A. D., M.-S. Yao, W. Kovari, and K. K.-W. Lo (1996), A prognostic cloud water parametrisation for global climate models, *J. Climate*, *9*, 270–304.

Dubuisson, P., V. Giraud, O. Chomette, H. Chepfer, and J. Pelon (2005), Fast radiative transfer modeling for infrared imaging radiometry, *J. Quant. Spectrosc. Radiat. Transfer*, *95*, 201–220.

Ghan, S. J., and R. C. Easter (1992), Computationally efficient approximations to stratiform cloud microphysics parameterization, *Mon. Wea. Rev.*, *120*, 1572–1582.

Ho, S.-P., B. Lin, P. Minnis, and T.-F. Fan (2003), Estimation of cloud vertical structure and water amount over tropical oceans using VIRS and TMI data, *J. Geophys. Res.*, *108*(D14), 4419, doi:10.1029/2002JD003298.

Hogan, R. J., M. D. Behera, E. J. O'Connor, and A. J. Illingworth (2004), Estimate of the global distribution of stratiform supercooled liquid water clouds using the LITE lidar, *Geophys. Res. Lett.*, *31*, L05106, doi:10.1029/2003GL018977.

Hu, Y. (2007), Depolarization ratio–effective lidar ratio relation: Theoretical basis for space lidar cloud phase discrimination, *Geophys. Res. Lett.*, *34*, L11812, doi:10.1029/2007GL029584.

Hu, Y. X., and K. Stamnes (1993), An accurate parameterization of the radiative properties of water clouds suitable for use in climate models. *J. Climate*, *6*, 728–742.

Hu, Y., D. Winker, P. Yang, B. Baum, L. Poole, and L. Vann (2001), Identification of cloud phase from PICASSO-CENA lidar depolarization: A multiple scattering sensitivity study. *J. Quant. Spectrosc. Radiat. Transfer*, *70*, 569–579.

Hu, Y., et al. (2006), A simple relation between lidar multiple scattering and depolarization for water clouds. *Opt. Lett.*, *31*, 1809–1811.

Hu, Y., M. Vaughan, C. McClain, M. Behrenfeld, H. Maring, D. Anderson, S. Sun-Mack, D. Flittner, J. Huang, B. Wielicki, P. Minnis, C. Weimer, C. Trepte, and R. Kuehn (2007a), Global statistics of liquid water content and effective number concentration of water clouds over ocean derived from combined CALIPSO and MODIS measurements, *Atmos. Chem. Phys.*, *7*, 3353–3359.

Hu, Y, M. Vaughan, Z. Liu, K. Powell, and S. Rodier (2007b), Retrieving Optical Depths and Lidar Ratios for Transparent Layers Above Opaque Water Clouds From CALIPSO Lidar Measurements, *Geosci. Remote Sens. Lett.*, *4*, 523–526.

Hu, Y., M. Vaughan, Z. Liu, B. Lin, P. Yang, D. Flittner, W. Hunt, R. Kuehn, J. Huang, D. Wu, S. Rodier, K. Powell, C. Trepte, and D. Winker (2007c), The depolarization-attenuated backscatter relation: CALIPSO lidar measurements vs. theory, *Optics Express*, *15*, 5327–5332.

Hu, Y., D. Winker, M. Vaughan, B. Lin, A. Omar, C. Trepte, D. Flittner, P. Yang, S. Nasiri, B. A. Baum, W. Sun, Z. Liu, Z. Wang, S. Young, K. Stamnes, J. Huang, R. Kuehn, and R. E. Holz (2009), CALIPSO/CALIOP cloud phase discrimination algorithm. *J. Atmos. Ocean. Technol.*, *26*, 2206–2309. DOI:10.1175/2009JTECHA1280.1.

Li, Z.-X., and H. Le Treut (1992), Cloud-radiation feedbacks in a general circulation model and their dependence on cloud modelling assumptions, *Clim. Dyn.*, *7*, 133–139.

Klein, S. A., et al. (2009), Intercomparison of model simulations of mixed-phase clouds observed during the ARM Mixed-Phase Arctic Cloud Experiment. I: Single-layered cloud. *Quart. J. Roy. Meteor. Soc.*, *135*, 979–1002.

Korolev, A. V., G. A. Isaac, J. W. Strapp, S. G. Cober, and H. W. Barker (2007), In situ measurements of liquid water content profiles in mid-latitude stratiform clouds, crystals in a supercooled water cloud, *Quart. J. Roy. Meteor. Soc.*, *133*, 1693–1699.

Lin, B., and W. B. Rossow (1994), Observations of cloud liquid water path over oceans: Optical and microwave remote sensing methods, *J. Geophys. Res.*, *99*, 20907–20927.

Lin, B., and W. B. Rossow (1996), Seasonal variation of liquid and ice water path in non-precipitating clouds over oceans, *J. Climate*, *9*, 2890–2902.

Mason, B. J. (1952), The growth of ice crystals in a supercooled water cloud, *Quart. J. Roy. Meteor. Soc.*, *79*, 104–111.

Nasiri, S. L., and B. H. Kahn (2008), Limitations of bi-spectral infrared cloud phase determination and potential for improvement. *J. Appl. Meteor. Clim.*, *47*, 2895–2910.

Smith, R. N. (1990), A scheme for predicting layer clouds and their water content in a general circulation model, *Quart. J. Roy. Meteor. Soc.*, *116*, 435–460.

Tao, W-K. (2003), Goddard cumulus ensemble (GCE) model: Application for understanding precipitation processes. *Meteorol. Monogr.*, *29*, 107–138.

Toon, O. B., C. P. McKay, T. P. Ackerman, and K. Santhanam (1989), Rapid calculation of radiative heating rates and photodissociation rates in inhomogeneous multiple scattering atmospheres. *J. Geophys. Res.*, *94*, 16287–16301.

Tsushima, Y., S. Emori, T. Ogura, M. Kimoto, M. J. Webb, K. D. Williams, M. A. Ringer, B. J. Soden, B. Li, and N. Andronova (2006), Importance of the mixed-phase cloud distribution in the control climate for assessing the response of clouds to carbon dioxide increase: a multi-model study. *Clim. Dyn.*, *27*, 113–126.

Weidle, F., and H. Wernli (2008), Comparison of ERA40 cloud top phase with POLDER-1 observations, *J. Geophys. Res.*, *113*, D05209, doi:10.1029/2007JD009234.

Winker, D. M., W. H. Hunt, and M. J. McGill (2007), Initial performance assessment of CALIOP. *Geophys. Res. Lett.*, *34*, L19803, doi:10.1029/2007GL030135.

Yin, J. (2005), A consistent poleward shift of the storm tracks in simulations of 21st century climate. *Geophys. Res. Lett.*, *32*, L18701, doi:10.1029/2005GL023684.

Y. Hu, J. Huang, D. Josset, B. Lin, S. Rodier, W. Sun, K. Xu, and P. Zhai, Climate Science Branch, NASA Langley Research Center, Hampton, VA 23681, USA. (yongxiang.hu-1@nasa.gov)